

A Modular and Integrated Optimisation Model for Underwater Vehicles

K.L. Vasudev[#], R. Sharma^{#,*}, and S.K. Bhattacharyya[#]

[#]Department of Ocean Engineering, Indian Institute of Technology Madras, Chennai-600 036, India

*E-mail: rajivatri@iitm.ac.in

ABSTRACT

A modular and integrated optimisation model for the design of underwater vehicles is presented. In the proposed optimisation model two modules (i.e. low fidelity and high fidelity) are incorporated and the basic geometric definition of computer aided design (CAD) is integrated with computational fluid dynamic (CFD) analysis. The hydrodynamic drag is considered as single objective with constraints on the geometric parameters of dimension, space and volume. The CAD model is implemented in MATLAB[™] and CFD model is implemented in Shipflow^{**™}. A real-world design example of an existing underwater vehicle is presented. The applicability of proposed optimisation model is shown. The presented results show that within given set or sets of constraints the application of optimisation model in design results into an efficient hull form.

Keywords: Hydrodynamic drag, genetic algorithm, computational fluid dynamics, computer aided design, underwater vehicles

NOMENCLATURE

c_f	Skin friction coefficient
c_p	Prismatic coefficient
C_{PV}	Viscous pressure drag coefficient
C_v	Viscous drag coefficient
d_{\max}	Maximum diameter, m
$d_{t\max}$	Maximum tail diameter, m
D	Hydrodynamic drag, N
L	Total length, m
L_m	Length of the parallel middle body, m
L_n	Length of nose, m
L_t	Length of the tail, m
n_n	Shape variation coefficient of nose
n_t	Shape variation coefficient of tail
r_n	Radius of nose, m
r_t	Radius of tail, m
S	Total wetted surface area, m^2
v	Velocity of the vehicle, m/s
v_x	Normalised axial velocity, m/s
ρ	Density of the fluid, kg/m^3
∇	Volume displacement, m^3

1. INTRODUCTION

The oceans have been always a fascination for humans. Although, roughly the ocean covers 71 per cent of the Earth's surface and contains 97 per cent of the planet's water, still around 95 per cent of the underwater world remains unexplored¹. The demand for natural resources, need to understand earth's weather patterns, protection of coast from adverse attacks and national defense have motivated the

research for exploration of the oceans at deeper water depths. For oceanographic explorations the researchers have relied upon underwater vehicles - submarines, manned/unmanned underwater vehicles, remotely operated vehicles, and ship towed instrumentation packages, etc. However, underwater vehicles have their limitations too, e.g. power either drawn by cable from mother ship or onboard power storage and limited or no control with free/self-propelling vehicles.

A proper utilisation of power allows the vehicles to travel larger distances, at deeper depths and with heavier payloads. This demands a shape of the hull that results into lower drag, lesser power, and other favorable features. Primarily, this work focuses on computing shape of a hull that can result into lower drag. Because of their importance the underwater vehicles (UVs) are being studied worldwide and many design and development teams are active since the last decade, Singh², *et al.*

Even though the UVs are critically important because of their potential applications in both civil and defense areas, their design process remains relatively less documented, less automated and suffers from proper integration with other areas of advancement. Essentially, the design of UVs is mission specific and it gets more and more complex with increasing demands of range, endurance, payload, operational flexibility, demands of navigational capabilities for deep and restricted water depths, energy efficiency and other special mission requirements. These requirements of design are essentially conflicting in nature so and a compromise needs to be made that caters to all the design requirements of these vehicles. This implies that the estimation of 'best' design satisfying all or a set of requirements is computed with optimisation techniques.

In industrial practices, the UV design process is

largely based on adhoc approaches with design governed by experience and rules of thumb. Only recently, the multidisciplinary design optimisation (MDO) based methods have been used to identify optimal designs³⁻⁵. In the design of UV, power considerations plays a major role because small improvement in hydrodynamic drag can result in a substantial saving in thrust requirement and significant improvement in achieving higher vehicle speeds or increase in endurance of the vehicle⁶⁻⁷. The present work is motivated by this premise.

The work focuses on minimisation of hydrodynamic drag for a vehicle within certain pre-defined bounds of constraints on volume and total length. The computation of drag requires repetitive analysis of the local flow field around the hull with the variation of different geometric design parameters. This can be achieved with the parametric variation of the hull form followed by testing them in a towing tank. Although it is possible it is a highly expensive and time-consuming approach. Furthermore, the basic economics of design does not allow testing more than three designs in a towing tank⁸. Herein, the CFD has an advantage of reducing the time and cost of each analysis but it is difficult to manually do the parametric variations of hull parameters. This shows the requirement to solve the design problem with a robust and automatic optimisation process integrated with CFD. Building upon the recent advances in the areas of computing, CAD, CFD, the researchers have started investigating integrated design methods of optimisation and some of these attempts have focused on ships⁹⁻¹⁰.

In earlier works, the optimisation methods were shown to be effective in identifying an optimal design¹¹, however in the design cycles the integration of basic geometric definition in CAD and hydrodynamic analysis with CFD was not there. This work attempts to fill this gap. This work builds upon the earlier work⁶ and extends and elaborates that work with the inclusion of design modules (i.e. high fidelity and low fidelity) in the environment of complete and seamless integration of CAD and CFD. The design approach is modular and the selection of a particular design/analysis module is user specific, e.g. the user can select either high fidelity or low fidelity or both. Similarly, the integration of CAD and CFD is modular and in future other modules too can be added, e.g. maneuvering analysis module. The modular design approach is as shown in Fig. 1. The flow chart of the complete optimisation process is depicted in Fig. 2. The selection of

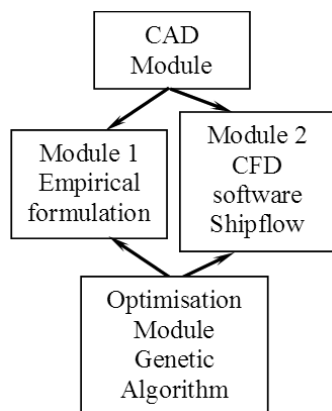


Figure 1. Modular and integrated optimisation framework.

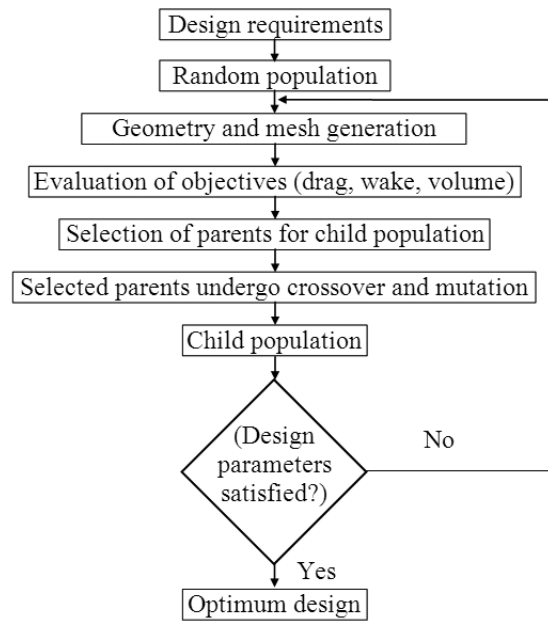


Figure 2. Flow chart of complete optimisation process.

design objectives considered in a particular design depends upon the requirements.

In this work, genetic algorithm (GA) is used to solve the optimisation problem. The GA's are better and more robust than conventional artificial intelligence (AI) methods¹²⁻¹³. Unlike older AI systems, the GA's do not break easily even if the inputs change slightly, or in the presence of reasonable noise¹⁴. The GA works efficiently for a large number of variables. This work considers a design objective (minimisation of hydrodynamic drag) and design parameters: length of nose, length of the parallel middle body, length of tail, maximum diameter, nose variation coefficient, and diameter of the tail.

2. BASIC FORMULATION OF DRAG

In this work the bare hull without any appendages and protrusions is considered. Although, it is a simplification because in actual design there are appendages, fins, and other protruding bodies, it is important to study bare hull because it forms the first step in any design optimisation process. Normally, the appendages add on to the naked/bare hull drag and their drags are defined as a fraction/percentage of naked/bare hull drag¹⁵, e.g. the in-service drag is defined:

$$D_{ser} = D_{nak} + D_{app} + D_{pro} + D_{ind} \quad (1)$$

where D_{ser} is in-service drag, D_{nak} is naked hull drag, D_{app} is appendage drag, D_{pro} is protrusion drag, and D_{ind} is induced drag. However, to account for appendages drag and interaction of hull and appendages, the integrated hull (i.e. appendages with bare hull) needs to be optimised separately to achieve a lower drag hull with appendages. This is not focused in the current paper. The cross-sectional parameters (i.e. d_{max} , n_n and $d_{t,max}$) are utilised to generate various shapes within the constraints of volume and space area. Following White¹⁶ and Van & Van¹⁷, the hydrodynamic drag is:

$$D = \frac{1}{2} \rho C_v v^2 S \quad (2)$$

where D is the hydrodynamic drag (N), ρ is the density of fluid (kg/m^3), S is the total wetted surface area (m^2), v is the velocity of the vehicle in m/s , and C_v is the viscous drag coefficient

2.1 Low fidelity

Following, ITTC (1957) the model-ship correlation line¹⁸:

$$c_f = \frac{0.075}{(\log_{10} Rn - 2)^2} \quad (3)$$

where Rn is the Reynolds number which is:

$$Rn = \frac{\rho v L}{\mu} \quad (4)$$

where L total length of the vehicle m , v is the velocity m/s and μ is the dynamic viscosity of the fluid kg/ms . In low fidelity module, the C_v is computed using Jackson¹⁹ and it is:

$$C_v = c_f \left[1 + 1.5 \left(\frac{d_{max}}{L} \right)^{\frac{3}{2}} + 7 \left(\frac{d_{max}}{L} \right)^3 + 0.002 (c_p - 0.6) \right] \quad (5)$$

where c_p is the prismatic coefficient:

$$c_p = \frac{\nabla}{\pi \left(\frac{d_{max}}{2} \right)^2 L} \quad (6)$$

where ∇ is the volume displaced m^3 . It can be noted here that though other empirical formulations are also available, but they are not used in the present work because they are based upon either the surface area or fullness/fineness ratio and do not consider the local shape fairing^{3,20}.

2.2 High Fidelity

In high fidelity module, the C_v is computed using CFD analysis with Shipflow^{**TM}. In Shipflow^{**TM}, the Reynolds-Averaged Navier-Stokes (RANS) equations based discretisation model is used to solve the momentum equations for the viscous fluid. In Shipflow^{**TM} turbulence is introduced using the $k-\omega$ Shear Stress Transport (SST) utilising the advantages of both the $k-\varepsilon$ and $k-\omega$ models. This $k-\omega$ SST model (Menter²¹) blends the $k-\omega$ model in the near wall region with the free stream independence of the $k-\varepsilon$ model in the far field and that blending makes it robust, accurate and most effective, for more details see TM²².

A no-slip condition which states that velocity of the fluid at a solid boundary is zero relative to the boundary is considered over the surface of the axisymmetric body. The upstream boundary of the domain is modelled as velocity inlet (inflow) and the downstream boundary is modelled as velocity outlet (outflow). All other boundaries of the three-dimensional rectangular domain are modelled to experience a wall with no shear condition. The boundary conditions considered in the present work are as shown in Fig. 3. From Fig. 3, it can be observed that the computational domain extends up to $0.7L$ upstream from the leading edge and up to $4.5L$ downstream from the trailing edge and $1.2L$ is assumed to be the height and width of the rectangular domain of axisymmetric body. The solution domain is found to be large enough to capture the entire viscous-inviscid interaction and the wake development. The

coupling between the pressure and velocity fields is achieved using Roe Flux differencing scheme. A second order upwind scheme for convection and the central differencing scheme for diffusion terms have been used. More detailed discussion on these methods can be found in manual²².

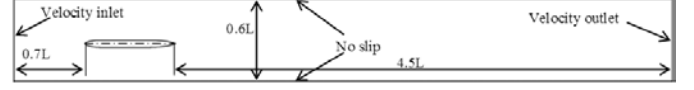


Figure 3. Fluid domain with boundary conditions for CFD calculations in high fidelity model.

Once the domain and the geometry are defined then meshing is done. Uniform mesh is generated along the body and the mesh is made finer near the body and coarser away from the body. The generated mesh comprises of hexahedral elements²³ and around 0.94 million are built from 0.84 million grid points. Since the $k-\omega$ SST turbulence model is used, the non-dimensional wall distance (y^+) is maintained in the range of 0 to 1 to capture the turbulence near the body wall. The generated mesh around the geometry is as shown in Fig. 4. In order to automate the mesh generation process scripting is done in Matlab^{*TM} and the generated files of Matlab^{*TM} are input files to Shipflow^{**TM}.

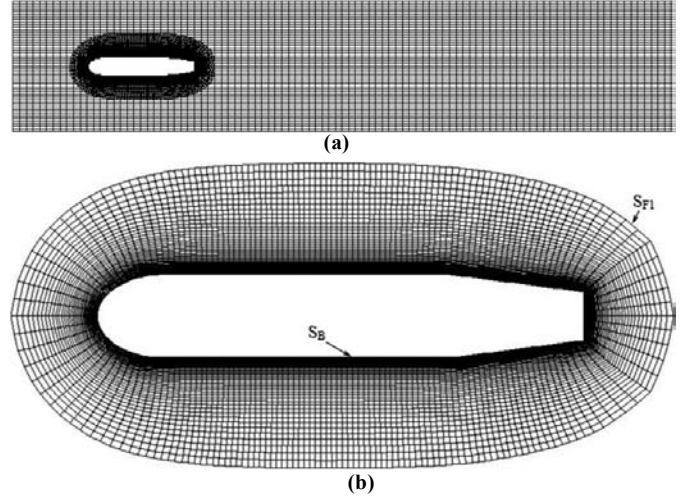


Figure 4. Mesh for toy submarine USS Dallas (No. of nodes 83500; no. of cells 956664) (a) Mesh in the full domain for toy submarine USS Dallas and (b) Mesh in the Q1 for toy submarine USS Dallas.

Primarily, in Shipflow^{**TM} the continuity equation in cylindrical coordinate for the flow past an axisymmetric underwater vehicle hull form is solved and it is:

$$\frac{\partial \rho}{\partial t} + \frac{\partial}{\partial x} (\rho v_x) + \frac{\partial}{\partial r} (\rho v_r) + \frac{\rho v_r}{r} = 0 \quad (7)$$

where x , r are the axial and radial coordinates respectively, v_x , v_r are the axial and radial velocity respectively, ρ is the density of the fluid kg/m^3 . The radial and axial momentum equations are:

$$\frac{\partial}{\partial t} (\rho v_r) + \frac{1}{r} \frac{\partial}{\partial x} (r \rho v_x v_r) + \frac{1}{r} \frac{\partial}{\partial r} (r \rho v_r v_r) = - \frac{\partial p}{\partial r} \quad (8)$$

$$\frac{\partial}{\partial t} (\rho v_x) + \frac{1}{r} \frac{\partial}{\partial x} (r \rho v_x v_x) + \frac{1}{r} \frac{\partial}{\partial r} (r \rho v_r v_x) = - \frac{\partial p}{\partial x} \quad (9)$$

where p is the static pressure and

$$\nabla \cdot \vec{v} = \frac{\partial v_x}{\partial x} + \frac{\partial v_r}{\partial r} + \frac{v_r}{r}. \quad (10)$$

The transport equations for k - ω SST model are:

$$\frac{\partial}{\partial t}(\rho k) + \frac{\partial}{\partial x_i}(\rho k u_i) = \frac{\partial}{\partial x_j} \left(\Gamma_k \frac{\partial k}{\partial x_j} \right) + \tilde{G}_k - Y_k \quad (11)$$

$$\frac{\partial}{\partial t}(\rho \omega) + \frac{\partial}{\partial x_i}(\rho \omega u_i) = \frac{\partial}{\partial x_j} \left(\Gamma_\omega \frac{\partial \omega}{\partial x_j} \right) + G_\omega - Y_\omega + D_\omega \quad (12)$$

where \tilde{G}_k is the generation of turbulence kinetic energy due to mean velocity gradients, G_ω is the generation of ω , $\Gamma_{k,\omega}$ represents the effective diffusivity of k and ω respectively, $Y_{k,\omega}$ represents the dissipation of k and ω respectively due to turbulence, and D_ω represents the cross-diffusion term.

3. OPTIMISATION PROBLEM FORMULATION

The optimisation problem treated in this paper consists of minimisation of drag subject to constraints on the geometric parameters. The problem may be stated as follows:

Minimize $F(x_1, x_2, \dots, x_6)$ subject to the constraints

$$x_1 + x_2 + x_3 \leq 0.35 \text{ m}; g(x_1, x_2, \dots, x_6) \geq c_g \quad (13)$$

and variable bounds

$$x_{Li} \leq x_i \leq x_{Ui} \quad (i = 1, 2, \dots, 6)$$

where

$$F = D, x_1 = L_n, x_2 = L_t, x_3 = L_m, x_4 = n, x_5 = r_{\max}, x_6 = r_t \quad (14)$$

$$g = \nabla, c_g = 0.000848 \text{ m}^3$$

and

$$x_{L1} = 0.04 \text{ m}, x_{L2} = 0.09 \text{ m}, x_{L3} = 0.21 \text{ m}, x_{L4} = 1,$$

$$x_{L5} = 0.025 \text{ m}, x_{L6} = 0.0175 \text{ m}, x_{U1} = 0.1 \text{ m}, x_{U2} = 0.15 \text{ m},$$

$$x_{U3} = 0.3 \text{ m}, x_{U4} = 3, x_{U5} = 0.035 \text{ m}, x_{U6} = 0.0225 \text{ m}. \quad (15)$$

The method used in solving the linear constraint problem is 'genetic algorithm for numerical optimisation for constrained problems (GENOCOP)'²⁴⁻²⁵. The method specialised to the problem given by Eqns. (13) - (15), will be discussed now in a step-by-step manner.

Step 1: Generation of initial population

A vehicle configuration $C^{(j)}$ is given by the parameter set $x_i^{(j)}$ ($i = 1, 2, \dots, 6$) Generate $6p$ random numbers, α_k ($k = i \times j$), with p even, between 0 and 1. Then, we generate p vehicle configurations $C^{(j)}$ ($j = 1, 2, \dots, p$) from these random numbers, using

$$x_i^{(j)} = x_{Li} + \alpha_k (x_{Ui} - x_{Li}) \quad (16)$$

We find the vehicle configurations. These configurations constitute the initial population. In the present work, $p = 10$ has been used in high fidelity model and $p = 50$ in low fidelity model. At the end of Step 1, we have p vehicle configurations.

Step 2: Evaluation of objective function for the initial population and ranking them

We compute the drag forces $F^{(j)}$ ($j = 1, 2, \dots, p$) of each of these p configurations $C^{(j)}$ ($j = 1, 2, \dots, p$) using CFD in high fidelity model and using empirical formulae in low fidelity

model. Also, compute the volumes of the configurations $g^{(j)}$ ($j = 1, 2, \dots, p$). Let the number of configurations which satisfy the inequality constraint $g^{(j)} \geq c_g$ (see Eqn. (14)) be p_1 . The number of configurations which do not satisfy it is then $p_2 = p - p_1$. Now, we reorder the configurations which satisfy the inequality constraint in the ascending order of their drag forces and denote it as $C_{R1}^{(j)}$ ($j = 1, 2, \dots, p_1$). The drag forces corresponding to $C_{R1}^{(j)}$ are $F_{R1}^{(j)}$ ($j = 1, 2, \dots, p_1$) and the volumes corresponding to $C_{R1}^{(j)}$ are $g_{R1}^{(j)}$ ($j = 1, 2, \dots, p_1$). For these p_1 configurations,

$$F_{R1}^{(j)} < F_{R1}^{(j+1)} \text{ and } g_{R1}^{(j)} \geq c_g \quad (j = 1, 2, \dots, p_1) \quad (17)$$

Also, we reorder the configurations which do not satisfy the inequality constraint in the descending order of their volumes and denote it as $C_{R2}^{(j)}$ ($j = 1, 2, \dots, p_2$). The drag forces corresponding to $C_{R2}^{(j)}$ are $F_{R2}^{(j)}$ ($j = 1, 2, \dots, p_2$) and the volumes corresponding to $C_{R2}^{(j)}$ are $g_{R2}^{(j)}$ ($j = 1, 2, \dots, p_2$). For these p_2 configurations,

$$g_{R2}^{(j)} > g_{R2}^{(j+1)} \text{ and } g_{R2}^{(j)} < c_g \quad (j = 1, 2, \dots, p_2) \quad (18)$$

Finally, we form a set of configurations $C_R^{(j)}$ ($j = 1, 2, \dots, p$)

by adding $C_{R1}^{(j)}$ ($j = 1, 2, \dots, p_1$) and $C_{R2}^{(j)}$ ($j = 1, 2, \dots, p_2$) sequentially, i.e.

$$C_R^{(j)} \quad (j = 1, 2, \dots, p_1) = C_{R1}^{(j)} \quad (j = 1, 2, \dots, p_1); \quad (19)$$

$$C_R^{(j)} \quad (j = p_1 + 1, p_1 + 2, \dots, p) = C_{R2}^{(j)} \quad (j = 1, 2, \dots, p_2)$$

At the end of *Step 2*, we have p vehicle configurations ordered in such a way that the first p_1 are in the ascending order of their drag forces and the last p_2 are in the descending order of their volumes. The ranking is done.

Step 3: Picking parent population and either crossover or mutation will be carried over the picked parent population

Consider the first $p/2$ configurations of $C_R^{(j)}$ (p even) and denote it $C_{RU}^{(j)}$, i.e.

$$C_{RU}^{(j)} \quad (j = 1, 2, \dots, p/2) = C_R^{(j)} \quad (j = 1, 2, \dots, p/2) \quad (20)$$

Generate a random number α between 0 and 1. If $\alpha \leq \bar{\alpha}$, where the chosen value of $\bar{\alpha} = 0.9$ in the present calculations, generate two random numbers β_1 and β_2 . If $\alpha > \bar{\alpha}$, generate a random number β . Then

(a) If $\alpha \leq \bar{\alpha}$, select two configurations

$C_{RU}^{(r)}$ and $C_{RU}^{(s)}$ ($r, s \in (1, 2, \dots, p/2)$) based on the random numbers β_1 and β_2 respectively using

$$\text{Configuration } r \text{ if } \frac{2(r-1)}{p} \leq \beta_1 \leq \frac{2r}{p}; \quad (21)$$

$$\text{Configuration } s \text{ if } \frac{2(s-1)}{p} \leq \beta_2 \leq \frac{2s}{p}$$

Then generate 6 random numbers γ_i ($i = 1, 2, \dots, 6$) and develop two new configurations as

$$\bar{C}^{(r)} : x_i = \frac{1}{2} \{ (1 - \gamma_i) x_i^{(r)} + (1 + \gamma_i) x_i^{(s)} \}; \quad (22)$$

$$\bar{C}^{(j+1)} : x_i = \frac{1}{2} \{ (1 + \gamma_i) x_i^{(r)} + (1 - \gamma_i) x_i^{(s)} \}$$

where $j-1$ is the number of $\bar{C}^{(j)}$ configurations already developed.

(b) If $\alpha > \bar{\alpha}$, then calculate

$$\begin{aligned} \delta &= (2\beta)^{\frac{1}{\eta+1}} + 1 \quad (\text{if } \beta < 0.5); \\ \delta &= 1 - [2(1-\beta)]^{\frac{1}{\eta+1}} \quad (\text{if } \beta \geq 0.5) \end{aligned} \quad (23)$$

where $\eta = 20$ has been used and develop a new configuration as

$$\bar{C}^{(j)} : x_i = x_i^{(r)} + \delta(x_{Ui} - x_{Li}) \quad (i = 1, 2, \dots, 5) \quad (24)$$

The steps 3(a) and 3(b) given by Eqns. (21), (22) and (23) are repeated till $j = p$. In other words, p new configurations, denoted $\bar{C}^{(j)}$ ($j = 1, 2, \dots, p$) are developed. We compute the drag forces $\bar{F}^{(j)}$ ($j = 1, 2, \dots, p$) of each of these p configurations $\bar{C}^{(j)}$ ($j = 1, 2, \dots, p$) using CFD in high fidelity model and empirical formulae in low fidelity model. Also, we compute the volumes of the configurations $\bar{g}^{(j)}$ ($j = 1, 2, \dots, p$).

Step 4:

We form a set of configurations $\hat{C}^{(j)}$ ($j = 1, 2, \dots, 2p$) by appending $C_R^{(j)}$ ($j = 1, 2, \dots, p$) and $\bar{C}^{(j)}$ ($j = 1, 2, \dots, p$) sequentially, i.e.

$$\begin{aligned} \hat{C}^{(j)} (j = 1, 2, \dots, p) &= C_R^{(j)} (j = 1, 2, \dots, p); \\ \hat{C}^{(j)} (j = p+1, p+2, \dots, 2p) &= \bar{C}^{(j)} (j = 1, 2, \dots, p) \end{aligned} \quad (25)$$

The drag forces and volumes of these $2p$ configurations are now known. Now, we reorder these configurations as was done in Step 2 (see Eqns. (17) - (19)), namely, the configurations which satisfy the inequality constraint on volume are arranged first in ascending order of their drag forces, followed by the configurations which do not satisfy the inequality constraint on volume are arranged in descending order of their volumes. This configuration set consisting $2p$ configurations are denoted $\hat{C}_R^{(j)}$ ($j = 1, 2, \dots, 2p$). Consider the first p configurations of $\hat{C}_R^{(j)}$ and denote it $\hat{C}_{RU}^{(j)}$, i.e.

$$\hat{C}_{RU}^{(j)} (j = 1, 2, \dots, p) = \hat{C}_R^{(j)} (j = 1, 2, \dots, p) \quad (26)$$

Re-designate $\hat{C}_{RU}^{(j)}$ as $C_R^{(j)}$ ($j = 1, 2, \dots, p$) and go to Step 3

for the next iteration till the drag force of the first configuration, i.e. $C_R^{(1)}$, does not decrease further with an assumed tolerance. This will then be the optimised configuration. Once the optimised configuration is achieved the iterations will still go on to make sure that it is the global optimal solution in the given range.

4. NUMERICAL IMPLEMENTATION

The single objective optimisation problem is formulated with minimisation of hydrodynamic drag as the objective function. The problem is solved in two modules, i.e. high fidelity module, and low fidelity module. The constraints on design variables along with constraints on the volume and total length and the design variables are same in both the modules. We consider only the practical and applicable range of L/d_{\max} ratios from 4.92 to 11. Table 1 shows the parameters of genetic algorithm used in the present work.

The real design parameters of an underwater vehicle

are difficult to find in the existing literature because of their defense related applications, e.g. submarine drag results are rare. Hence, we adopt a scale-down approach. To demonstrate the applicability of our design approach we select a highly complex underwater vehicle – submarine – but select a scaled down version of it – toy submarine²⁶. It has advantages: in open literature research results are available about a toy submarine⁵, the complexity levels are same, and benchmarking of the results is possible. The design requirements chosen in this study are the same as the design requirements considered in Alam⁵, *et al.*, i.e. speed is 0.5 m/s, and overall length no longer than 350 mm, and cost effectiveness.

Table 1. The genetic algorithm parameters used in the present work

Parameter	Value
No. of variables	5
Population size	10
Crossover rate	0.9
Mutation rate	0.1
No. of generations	19
No. of evaluations	190

After, considering the basic design requirements, the geometry selection for UV is formulated:

Hull geometry: The hull size of toy UV is constrained by the space requirements to carry on board instruments and it needs to be minimised for drag. The parameterisation of hull geometry is as shown in Fig. 5. The nose radius is:

$$r_n = \frac{d_{\max}}{2} \left(1 - \left(\frac{(x - L_t - L_m)}{L_n} \right)^{n_n} \right)^{1/n_n} \quad (27)$$

Depending on the value of n_n the nose shape can vary from the conical nose for $n_n = 1$ and fuller and bulkier nose for large values of n_n . The tail-section considered in this work is a frustum with a diameter d_{\max} on one side of the frustum and diameter $d_{t\max}$ on the other side. Similar to nose the frustum can also vary between conical tail for $d_{t\max} = 0$ and rectangular tail for $d_{t\max} = d_{\max}$. But, in the present work the minimum and maximum bounds on n_n and $d_{t\max}$ are set as $1 \leq n_n \leq 3$ and $35 \leq d_{t\max} \leq 45 \text{ mm}$.

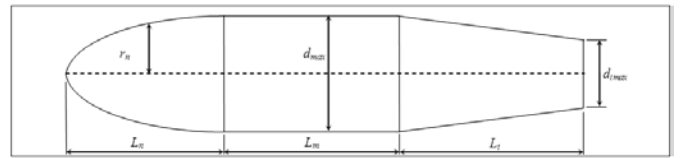


Figure 5. Parameterisation of the hull geometry of USS Dallas.

5. RESULTS AND DISCUSSIONS

5.1 Low Fidelity Model

The results of low fidelity model are listed in Tables 2 and 3 and the shape variation is as shown in Fig. 6. We can observe from Fig. 6 that the optimum designs – both by the low and high fidelity models – have fuller noses as compared to the parent hull of USS Dallas.

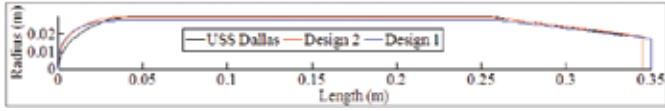


Figure 6. Shape comparison between USS Dallas, Design 1 (Optimum in low fidelity) and Design 2 (Optimum in high fidelity).

This result of a fuller nose resulting into still a lower drag is against the conventional practice in design wherein a finer nose is assumed to result into a favourable drag. Our result shows that this is not always true as a fuller nose might result into a higher skin frictional drag but the fairing of the nose with respect to the overall length determines the fluid velocity over the body and that affects the pressure drag. A nose with high skin friction can also result into lower pressure drag and this is precisely captured by both the optimisation models. A fuller nose has better design applications because it offers larger volume and better space to the sensors and systems that are placed in the nose section.

Table 2 shows the comparison between the USS Dallas, Design 1 and Design 2. Figs. 7(a) - 7(b) shows the variation in fitness function (i.e. hydrodynamic drag) and volume constraint in the optimisation process using low fidelity model. It is clear from the figures that after around 20 - 25 generations the fitness value does not change significantly and the solutions converge to the minimum of drag. The difference in surface area of Design 1 and parent hull of USS Dallas is almost insignificant and their lengths are same, as a result, there is no significant change in skin friction drag. Although, the viscous pressure coefficient can change for Design 1 and parent hull as depends heavily on the local shape variation of hull form, the empirical formulations do not account for shape variation effect. This lack of ability to include the local shape variation is a serious restriction of low fidelity models.

As mentioned, this limitation of the absence of local shape variation in low fidelity models is studied by us in detail. In our work, after computing the optimum, the hull forms of both – Design 1 and Design 2 - are analysed for the drag using CFD for different velocities ranging from 0.5 – 2.0 m/s, as in CFD one can visualise the local variation of flow along and around the body. These results are presented in Table 3.

From Table 2, we can see that a reduction in maximum diameter raises the slenderness ratio of the body from 5.83 for parent hull to 6.25 for Design 1. The total wetted surface area of the optimum hull is reduced from 0.0612 to 0.0585 by 4.4% and this results in the reduction of skin friction coefficient from 0.00714 of parent hull to 0.0062 of Design 1 by 13.2%. The difference in drag estimation between the empirical formulations based and CFD based is more than 50%. Since, slowly CFD computations are gaining better accuracy, the empirical formulations tend to become less reliable and accurate.

However, the difference of drag between parent and optimum hull even with a low fidelity model proves the efficiency of using an optimisation model to obtain an optimised hull for low drag.

5.2 High Fidelity Model

The results of high fidelity model are presented in Table 2 and Table 3 along with low fidelity model results. Figs. 8(a) - 8(b) show the variation in fitness function (i.e. hydrodynamic drag) and the volume constraint with subsequent iteration (i.e. generations) in high-fidelity optimisation model. It is clear from the figures that after 12 generations the fitness value is not varying significantly and the solution is converging to the minimum value of drag. Figs. 9(a) - 9(c) presents the normalised axial velocity (Velocity X (v_x) = v_x/v) contours over

Table 2. The comparison of hull parameters of USS Dallas, Design 1 and Design 2

Vehicle particulars	Parent hull (USS Dallas)	Design 1*	Design 2**
L_n, mm	45	44	43
L_m, mm	210	216	211
L_t, mm	95	90	91
L, mm	350	350	345
n_n	1.9	2.83	2.43
d_{max}, mm	60	56	59
d_{tmax}, mm	35	35	37
L / d_{max}	5.8	6.25	5.8
S, m^2	0.0612	0.0585	0.0611
∇, m^3	0.000848	0.000848	0.000848
$v, m/s$	0.5	0.5	0.5
$\rho, kg/m^3$	1000	1000	1000
Computation based upon empirical formulations of Equations (3, 5)			
c_f	0.00713	0.007139	0.0071
C_v	0.00803	0.00829	0.0081
$C_{pv} = C_v - c_f$	0.00088	0.001154	0.000999
$C_{PV} (\% C_v)$	10.9%	13.9%	12.3%
Drag (D), N	0.06144	0.0607	0.0610
Reduction in drag, %	-	1.2	0.78
Drag per unit volume	72.5	71.5	71.93
Reduction, %	-	1	0.78
Computations based upon CFD			
c_f	0.00714	0.0062	0.00717
C_v	0.01261	0.01235	0.01165
$C_{pv} = C_v - c_f$	0.00547	0.0061	0.00448
$C_{PV} (\% C_v)$	43.4%	49.4%	38.5%
Drag (D), N	0.0965	0.0945	0.0871
Reduction in drag, %	-	2.1	9.8
Drag per unit volume	113.8	111.43	102.7
Reduction, %	-	2.1	9.8

Design 1*: Computed optimum with low fidelity optimisation model; and Design 2**: Computed optimum with high fidelity optimisation model.

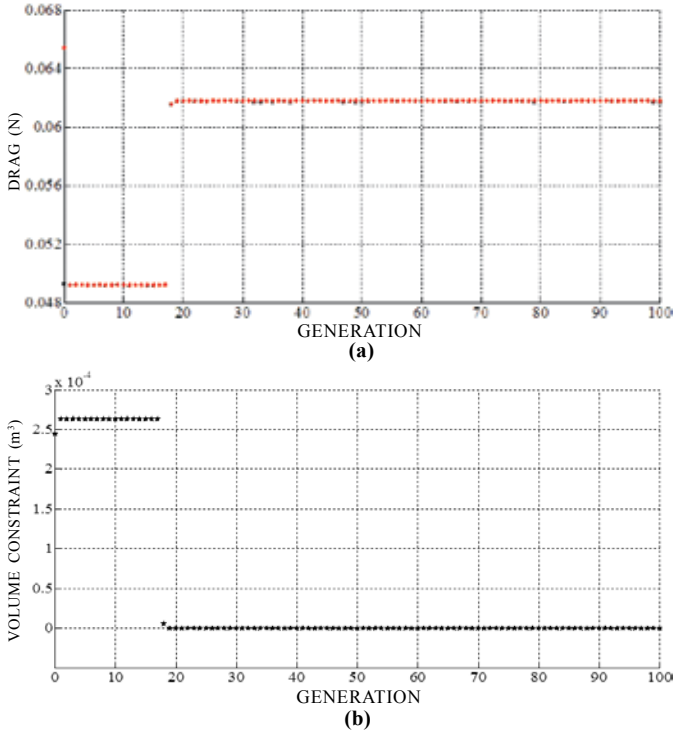


Figure 7. (a) Progress plot of the objective function (Hydrodynamic drag) in low fidelity model, and (b) Progress plot of the volume constraint in low fidelity model.

the hull forms of parent USS Dallas, Design 1 (in low fidelity model) and Design 2 (in high fidelity model) for velocity, $v=0.5$ m/s. If a body is covered with the low v_x that implies that the axial component of fluid flow velocity over the body is low and it will need thrust to move forward against the fluid flow resulting in lower drag or resistance.

A careful examination of Figs. 9 (a), 9(b), and 9(c) reveals that the Design 2 is covered with low v_x (i.e. close to 0) as compared to the v_x of around 0.111 for the USS Dallas and Design 1. And, this low v_x results in lowest drag for the Design 2 among the three design optimums, USS Dallas, Design 1 and Design 2.

From Table 2, it is clear that the total length of Design 2 is reduced along with the maximum diameter. The difference in the total drag is not so significant because of the small size of the body. The reduction is proved to be 2.5% in drag. The Design 2 results in better performance as compared to

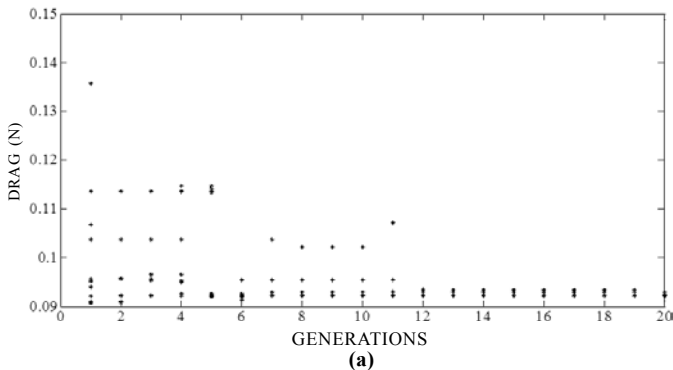


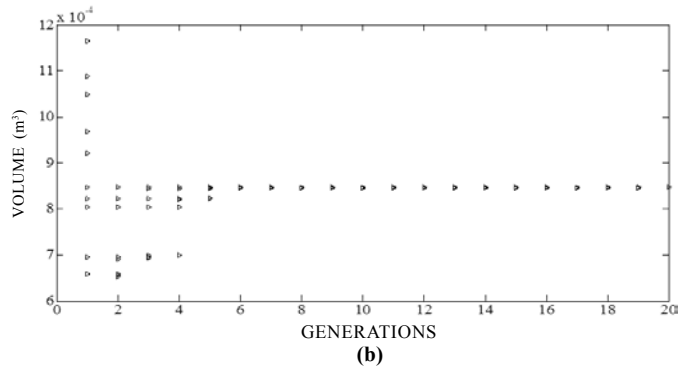
Figure 8. (a) Progress plot of the objective function (Hydrodynamic drag) in high fidelity model and (b). Progress plot of the volume constraint in high fidelity model.

Table 3. Comparison of drag computed using CFD for different velocities of USS Dallas, Design 1 and Design 2

v (m/s)	Computations based upon CFD	USS Dallas	Design 1*	Design 2**
1.0	C_{PV}	0.005977	0.005998	0.005977
	c_f	0.006163	0.006002	0.005093
	C_v	0.01214	0.012	0.01107
	C_{PV} (% C_v)	49.2%	49.9%	53.9%
	Drag (D) N	0.372	0.358	0.324
	Reduction %	-	3.5	12.8
1.5	C_{PV}	0.005424	0.005424	0.005443
	c_f	0.006346	0.005276	0.005057
	C_v	0.01177	0.0107	0.0105
	C_{PV} (% C_v)	46.1%	50.7%	51.8%
	Drag (D) N	0.811	0.704	0.706
	Reduction %	-	13.08	12.9
2.0	C_{PV}	0.005077	0.005077	0.005094
	c_f	0.006433	0.005493	0.005206
	C_v	0.01151	0.01057	0.0103
	C_{PV} (% C_v)	44.1%	48%	49.5%
	Drag (D) N	1.410	1.23	1.23
	Reduction %	-	12.2	12.2

Design 1*: Computed optimum with low fidelity optimisation model; and Design 2**: Computed optimum with high fidelity optimisation model.

the parent hull USS Dallas. The framework is proved to be useful by computing low drag hull forms compared to the existing parent hull form. In our opinion, the lesser length of the optimum hull in the high-fidelity model can result in lesser constructional costs and lesser drag results in low operational



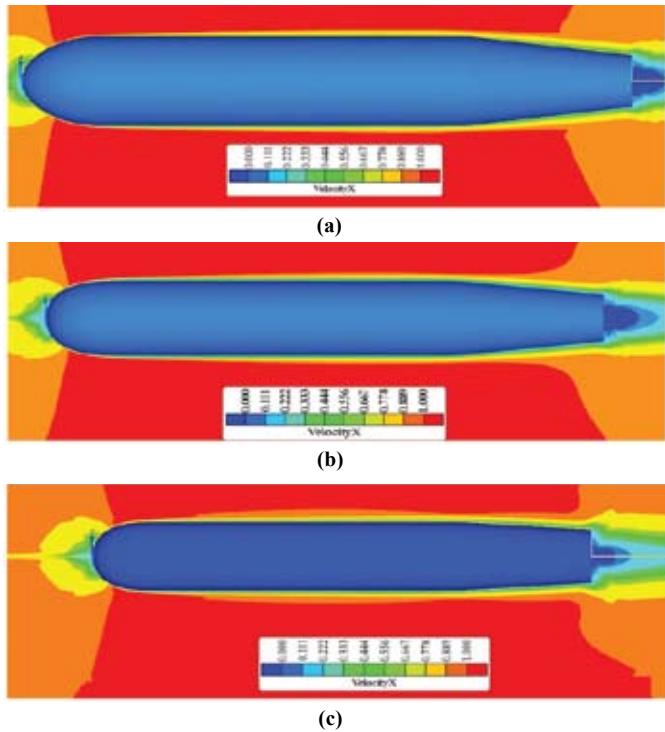


Figure 9. Normalised axial velocity (Velocity X = v_x/v) contours around (a) USS Dallas, (b) Design 1 and (c) Design 2 for $v=0.5$ m/s.

costs of the RC toy. Furthermore, we can observe from Table 3 that both Design 1 and Design 2 are performing better than the existing USS Dallas even for different velocities.

Figures 10 (a) - 10 (c) present the pressure distribution along the hull forms of parent USS Dallas, Design 1 and Design 2 for a velocity of 0.5 m/s. From the figures, it is clear that most of the hull form of USS Dallas is covered with a total pressure coefficient of -0.033 to -0.189 whereas in the case of Design 1 and Design 2 these values are in between 0.122 and -0.033 . This reduces the viscous pressure coefficient of the hydrodynamic drag. Table 2 brings out this difference in viscous pressure drag coefficient very clearly, from 0.00547 in USS Dallas to 0.0061 in Design 1 and to 0.00448 in Design 2. And, this difference in viscous pressure drag coefficient results in the reduction of the total drag of hull forms.

However, the practical problem of using CFD is that it consumes a lot of time compared to low fidelity model. The low fidelity model based optimisation can be used as an initial estimate of the optimum to fix the bounds on the design variables for the high fidelity model based optimisation or it can even be handy during the initial stages of design of these underwater vehicles where no computational resources are available and time is less to report. If design development cycle time is not a constraint and computational resources are available, then it is obvious that the high fidelity model computes a better and efficient hull form as compared to low fidelity model.

6. CONCLUSIONS

Two optimisation design frameworks (i.e. low fidelity and high fidelity) for the design of UVs are presented. In

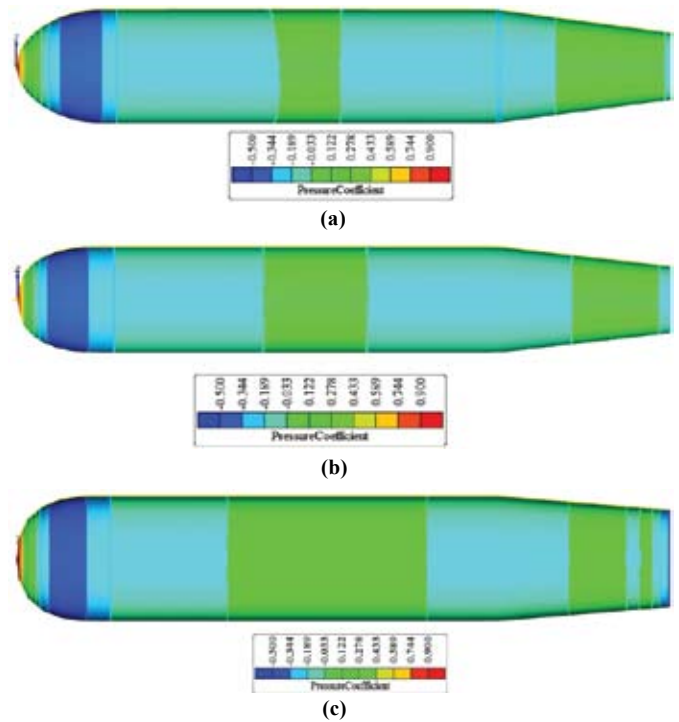


Figure 10. Total pressure coefficient contours over: (a) USS Dallas, (b) Design 1 and (c) Design 2 for $v = 0.5$ m/s.

low fidelity model, the objective function is evaluated using empirical formulations and in high fidelity model it is evaluated using CFD. We have shown that the low fidelity model based optimisation design framework is less accurate but consumes very less computational time when compared to the high fidelity model based optimisation design framework. Both of the optimisation methods have been implemented on RC toy submarine USS Dallas and they showed their efficacy in finding the optimum designs.

Our presented results show the effectiveness of shape parameters in the design of UVs. Since the presented example is of RC toy which is of a very short length, the results show less improvement. For larger UVs at higher speeds, the improvements will be higher and that will result into efficient designs. However, in the present work the optimisation has been restricted to only drag and volume. In a real design process, other criteria (e.g. dynamics of the vehicle, control with fins, hotel loads, internal arrangements, navigational and sensing requirements) also influence the final design. It will be interesting to investigate the extension of the present parametric driven modular optimisation design framework to account for other criteria. Additionally, a hull form for minimum drag is not always the best form for power, e.g. for a self-propelled body low drag does not necessarily reduce the thrust required as the effect of wake also plays an important role, Inoue¹⁷. A designer needs to focus on both, low drag as well as high wake fraction value. In the present work, we considered only hydrodynamic drag as objective no emphasis is given on wake fraction. Our further works will aim to addresses the role of power and other design requirements and currently some of our work is going in these directions.

REFERENCES

1. NOAA, Ocean, 2014. website address: <http://www.noaa.gov/ocean.html>
2. Singh, H.; Yoerger, D. & Bradley, A. Issues in AUV design and deployment for oceanographic research. *In* Proceedings - IEEE International Conference on Robotics and Automation, Albuquerque, New Mexico, 1997. doi: 10.1109/robot.1997.619058
3. Martz, M.A. Preliminary design of an autonomous underwater vehicle using a multiple-objective genetic optimizer. Virginia Polytechnic Institute and State University, Blacksburg, VA, 2008. M.S. Thesis.
4. Bertram, V. & Alvarez, A. Hydrodynamic aspects of AUV design. 5th conference on computer and IT applications in the maritime industries (COMPIT), Oegstgeest, Netherlands, 2006.
5. Alam, K.; Ray, T. & Anavatti, S.G. A new robust design optimization approach for unmanned underwater vehicle design. *Proc. Inst. Mech. Eng. Pt M: J. Eng. Maritime Environ.*, 2012, **226**(3), 235-249. doi: 10.1177/1475090211435450
6. Vasudev, K.L.; Sharma, R. & Bhattacharyya, S.K. A multi-objective optimization design framework integrated with CFD for the design of AUVs. *Methods Oceanography*, 2014, **10**, 138-165. doi: 10.1016/j.mio.2014.08.002
7. Alvarez, A.; Bertram, V. & Gualdesi, L. Hull hydrodynamic optimization of autonomous underwater vehicles operating at snorkeling depth. *Ocean Eng.*, 2009, **36**(1), 105-112. doi: 10.1016/j.oceaneng.2008.08.006
8. Kracht, A.M. Design of Bulbous Bows. *Transactions SNAME*, 1978a, 86, 197 – 217
9. Campana, E.F.; Peri, D.; Tahara, Y. & Stern, F. Shape optimization in ship hydrodynamics using computational fluid dynamics. *Comput. Methods Appl. Mech. Eng.*, 2006, **196**(1-3), 634-651. doi: 10.1016/j.cma.2006.06.003
10. Shahid, M. & Huang, D.B. Computational fluid dynamics based bulbous bow optimization using a genetic algorithm. *J. Marine Sci. Appl.*, 2012, **11**(3) 286-294. doi: 10.1007/s11804-012-1134-1
11. Parsons, J.S.; Goodson, R.E. & Goldschmied, F.R. Shaping of axisymmetric bodies for minimum drag in incompressible flow. *Journal Hydronaut*, 1974, 8, 100–107. doi: 10.2514/3.48131
12. Deb, K. An efficient constraint handling method for genetic algorithms. *Comput. Methods Appl. Mech. Eng.*, 2000, **186**(2-4), 311-338. doi: 10.1016/S0045-7825(99)00389-8
13. Deb, K.; Pratap, A.; Agarwal, S. & Meyarivan, T. A fast and elitist multiobjective genetic algorithm: NSGA-II. *IEEE Trans. Evol. Comput.*, 2002, **6**(2), 182-197. doi: 10.1109/4235.996017
14. Sivanandam, S.N. & Deepa, S.N. Introduction to genetic algorithms. Springer, Berlin, Germany, 2008, pp. 442.
15. Phillips, A.B.; Turnock, S.R. & Furlong, M. The use of computational fluid dynamics to aid cost-effective hydrodynamic design of autonomous underwater vehicles. *Proc. Inst. Mech. Eng. Pt M: J. Eng. Maritime Environ.*, 2010, **224**(4), 239-254. doi: 10.1243/14750902jeme199
16. White, F. Fluid Mechanics. Ed. 7. McGraw-Hill, USA, 2010. 885 p.
17. Van, Manen J.D. & Van, Oossanen P. Resistance. *In* The principles of Naval Architecture, edited by Edward v. Lewis, SNAME, USA, 1988. pp. 11-135.
18. ITTC, ITTC – Recommended Procedures: Testing and Extrapolation Methods Propulsion, Performance Propulsion Test. 2002, website address: itc.info/downloads/Archive%20of%20recommended%20procedures/2002%20Recommended%20Procedures/7.5-02-03-01.1.pdf (accessed on 15 May 2015)
19. Jackson, H. Submarine Design Trends. MIT Professional Summer Course, 1992.
20. Gillmer, T.C. & Johnson, B. Introduction to naval architecture. Ed. 2. US Naval Institute Press, USA, 1982. doi: 10.1007/978-94-011-6039-1
21. Menter, F.R. Zonal two equation $k-\omega$ turbulence models for aerodynamic flows. *In* 24th Fluid Dynamics Conference, Orlando, AIAA Paper 93-2906, July 1993.
22. TM Shipflow Xchap theoretical manual. FLOWTECH International AB, Sweden, 2007.
23. AFEM, Advanced Finite Element Methods, Department of Aerospace Engineering Sciences, University of Colorado at Boulder, USA, 2013. website: [www.colorado.edu/engineering / CAS courses.d/AFEM.d/](http://www.colorado.edu/engineering/CAS/courses/d/AFEM.d/) (accessed on 15 May 2015)
24. Miettinen, K.; Makela, M.M. & Toivanen, J. Numerical comparison of some penalty-based constraint handling techniques in genetic algorithms. *J. Global Optim.*, 2003, **27**(4), 427-446. doi: 10.1023/A:1026065325419
25. Rao, S.S. Optimization theory and applications. Wiley Eastern Limited, New Delhi, 1979, pp. 711.
26. AH, About Home - RC toys, 2015, website address: <http://rcvehicles.about.com> (accessed on 15 May 2015)

ACKNOWLEDGMENTS

This research was supported by the internal research grants of IIT Madras, Chennai, India through research scheme: OE10D010 and partially from Marine Systems Panel, NRB, DRDO, MoD, GoI, India via a sponsored project: NRB-263/MAR/12-13.

TRADEMARKS AND COPYRIGHTS

*Trademark and copyright with MathWorks, Inc., USA; and **Trademark and copyright with FLOWTECH International AB, Sweden.

CONTRIBUTORS

Mr K. L. Vasudev received his MTech Dual Degree in Naval Architecture from Saint Petersburg State Marine Technical University, Saint Petersburg, Russia in 2010 and recently he has submitted his PhD thesis on 'Hydrodynamic Optimization of Underwater Vehicles using Genetic Algorithm Integrated with CFD' to the Indian Institute of Technology Madras, India. His research interests includes: Optimization techniques in engineering, computational fluid dynamics and marine robotics.

Dr R. Sharma received his BE (Civil Engineering) from the Indian Institute of Technology, Roorkee (formerly University of Roorkee, Roorkee) in 1994; MTech (Ocean Engineering) in 1999 and PhD (Computer Aided Design and Manufacturing) from the Indian Institute of Technology Kharagpur, India in 2008. Presently, he is working as Associate Professor at the Department of Ocean Engineering, Indian Institute of

Technology Madras, Chennai, India. His research interests includes: Computer aided geometric design, computational geometry, visualisation, and their applications in design, manufacturing and robotics; ship production management and dynamic data driven forecasting systems.

Prof. S. K. Bhattacharyya received his BTech (H) (Naval Architecture) from the Indian Institute of Technology Kharagpur, in 1978; and MS and PhD in Ocean Engineering from the Indian Institute of Technology Madras, Chennai, India in 1985 and 1989, respectively. Presently, he is working as Professor at the Department of Ocean Engineering, Indian Institute of Technology Madras, Chennai, India. His research interests includes: Computer aided analysis of ship and offshore structures; ship structures, marine hydrodynamics and dynamics of floating bodies.